You might find this additional information useful...

Supplemental material for this article can be found at:
http://jn.physiology.org/cgi/content/full/00526.2007/DC1

This article cites 58 articles, 28 of which you can access free at:
http://jn.physiology.org/cgi/content/full/99/1/187#BIBL

Updated information and services including high-resolution figures, can be found at:
http://jn.physiology.org/cgi/content/full/99/1/187

Additional material and information about *Journal of Neurophysiology* can be found at:
http://www.the-aps.org/publications/jn

This information is current as of March 2, 2009 .

Transient Activity Induces a Long-Lasting Increase in the Excitability of Olfactory Bulb Interneurons

Tsuyoshi Inoue and Ben W. Strowbridge
Department of Neurosciences, Case Western Reserve University, Cleveland, Ohio

Inoue T, Strowbridge BW. Transient activity induces a long-lasting increase in the excitability of olfactory bulb interneurons. *J Neurophysiol* 99: 187–199, 2008. First published October 24, 2007; doi:10.1152/jn.00526.2007. Little is known about the cellular mechanisms that underlie the processing and storage of sensory in the mammalian olfactory system. Here we show that persistent spiking, an activity pattern associated with working memory in other brain regions, can be evoked in the olfactory bulb by stimuli that mimic physiological patterns of synaptic input. We find that brief discharges trigger persistent activity in individual interneurons that receive slow, subthreshold oscillatory input in acute rat olfactory bulb slices. A 2-to 5-Hz oscillatory input, which resembles the synaptic drive that the olfactory bulb receives during sniffing, is required to maintain persistent firing. Persistent activity depends on muscarinic receptor activation and results from interactions between calcium-dependent afterdepolarizations and low-threshold Ca spikes in granule cells. Computer simulations suggest that intrinsically generated persistent activity in granule cells can evoke correlated spiking in reciprocally connected mitral cells. The interaction between the intrinsic currents present in reciprocally connected olfactory bulb neurons constitutes a novel mechanism for synchronized firing in subpopulations of neurons during olfactory processing.

INTRODUCTION

The olfactory bulb is the second-order olfactory brain region, connecting olfactory sensory neurons in the nasal epithelium with the olfactory cortex (Shepherd and Greer 1998). Mitral cells, the excitatory principal neurons of the olfactory bulb, are inhibited by granule cells through reciprocal dendrodendritic synapses (Fig. 1*A*) (Isaacson and Strowbridge 1998; Jahr and Nicoll 1980; Rall et al. 1966). In addition to containing these unusual dendrodendritic synaptic connections, the olfactory bulb has long been appreciated as a site where large-amplitude synchronized oscillations can be recorded (Adrian 1942). Two principle types of synchronized oscillations are found frequently in the olfactory bulb: fast (~40 Hz) oscillations (Eeckman and Freeman 1990) proposed to be involved in odor discrimination (Stopfer et al. 1997) and slower (2–5 Hz) rhythms associated with sniffing and normal breathing (Freeman and Skarda 1985; Macrides and Chorover 1972 Ravel et al. 1987). These two types of oscillations differ in the phase relationships between mitral and granule cell activity during the oscillation. Freeman and colleagues found that local inhibitory interneurons discharged 90° out-of-phase with mitral cells during fast oscillations (Eeckman and Freeman 1990). In contrast, during slow oscillations, responses in both cell types are synchronized with no phase lag (Ravel et al.

1987). Despite evidence that sniffing behaviors are strongly modulated by behavioral states (Welker 1964), little is known about the significance of slow oscillations to the olfactory bulb computation.

Slow oscillations in the olfactory bulb may reflect a timing signal that is necessary to generate prolonged periods of synchronized firing in subpopulations of principal cells in response to transient olfactory stimuli. The underlying basis of oscillation-driven persistent activity (a firing mode triggered by a transient input that causes neurons to fire during most cycles in a previously subthreshold membrane potential oscillation) in the olfactory bulb may, therefore, be similar to the more intensively studied cortical forms of persistent activity (Compte et al. 2000; Goldman-Rakic 1995). Indeed, both olfactory (Ravel et al. 1992, 1994) and spatial (Everitt and Robbins 1997) working memory tasks are strongly modulated by muscarinic receptor activation. In some brain areas (e.g., entorhinal cortex (Egorov et al. 2002), lateral habenula (Wilcox et al. 1988)), individual neurons can become persistently active because they express specific combinations of intrinsic currents. In other brain areas, persistent activity is an emergent feature of the local circuit (Wang 2001) or interregional (Destexhe et al. 1999; McCormick and Bal 1997) connectivity. Aside from one report on persistent spiking in Blanes cells (Pressler and Strowbridge 2006), little is known about whether persistent activity exists in the olfactory bulb itself and how this activity would be regulated.

We approached this question by attempting to mimic the normal phasic synaptic input that olfactory bulb neurons receive from olfactory receptor neurons during attentive sniffing (Cang and Isaacson 2003; Chaput 2000; Margrie and Schaefer 2003). This periodic synaptic input likely contributes to the patterning of mitral cell discharges during olfactory responses (Chaput and Holley 1980; Macrides and Chorover 1972; Sobel and Tank 1993). Intracellular recordings demonstrate that the membrane potential of both mitral cells (Margrie and Schaefer 2003) and granule cells (Cang and Isaacson 2003) oscillate in response to the slow periodic synaptic input olfactory receptor neurons receive during sniffing, presumably with only a very small phase shift corresponding to the delay due to the mitral-to-granule cell excitatory synapse. We employed slow, subthreshold sinusoidal current stimuli to simulate these membrane potential oscillations in granule cells recorded in rat olfactory bulb slices. We found that granule cells became persistently active after a single excitatory stimulus in carbachol (CCh). This form of persistent activity was caused by
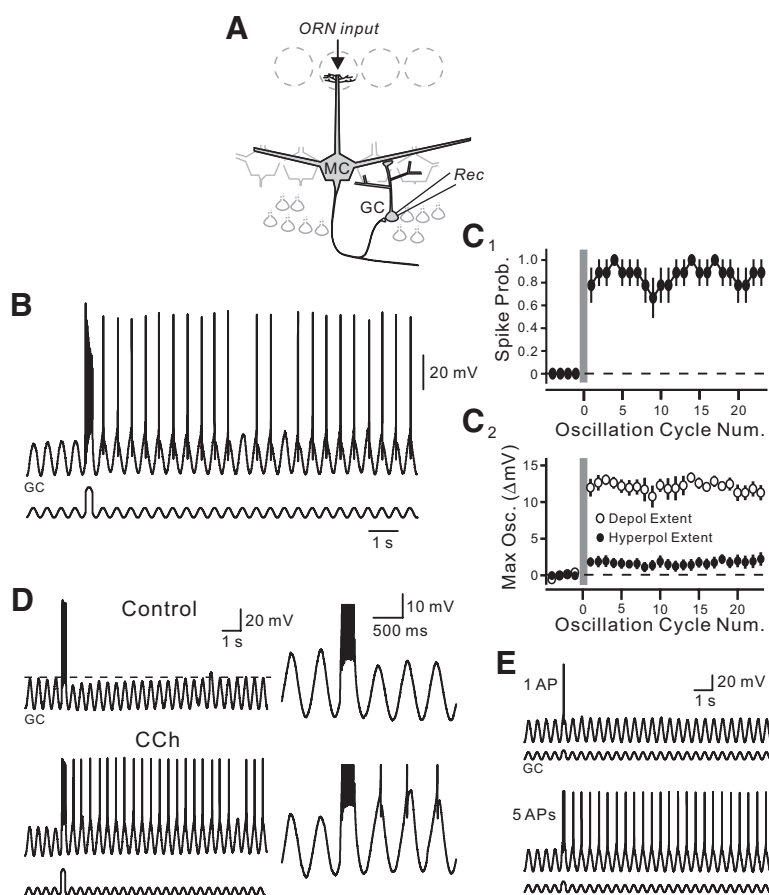

FIG. 1. Transient discharges trigger persistent firing in oscillating granule cells. *A*: schematic diagram of the olfactory bulb circuitry. *B*: persistent spiking evoked by a brief depolarizing stimulus in a granule cell injected with a subthreshold 2-Hz sinusoidal current waveform. Bath solution contained 1 μM carbacholCCh. *C1*: summary plot of average spiking activity in 9 granule cells tested with the stimulus protocol shown in *B*. *C2*: effect of transient discharge on the depolarizing (○) and hyperpolarizing (●) extent of the membrane potential oscillation. Plot shows relative change in oscillation extent after the stimulus. Action potentials removed using moving median filter. *D*: CCh-sensitive afterhyperpolarization prevents the transient discharge from triggering persistent spiking in oscillating granule cells. Expanded responses (*right*) show action potentials triggered by facilitated low-threshold spikes in CCh after the transient discharge. *E*: burst discharges (5 spikes; *bottom trace*) but not single spikes (*top trace*) trigger persistent firing in granule cells.

facilitated low-threshold Ca spikes triggered by Ca-dependent afterdepolarizations. These intrinsic conductances enable persistent firing to be initiated by a single, brief stimulus in granule cells that also receive a source of phasic input. Computer simulations suggest that persistent activity in granule cells can trigger correlated spiking in mitral cells and may function to synchronize firing in subpopulations of these output neurons during attentive olfactory tasks.

METHODS

Experimental methods

Horizontal slices (300 μm thick) of the main olfactory bulb were prepared from anesthetized (ketamine; 150 mg/kg ip) Sprague-Dawley rats (14–21 days old) using a vibrating tissue slicer. Slices were kept submerged in a holding tank that was maintained initially at 30°C for 30 min and then at room temperature. Electrophysiological and optical recordings were performed in a submerged recording chamber perfused with artificial cerebrospinal fluid (ACSF), the composition of which was (in mM) 124 NaCl, 2.5 KCl, 1.23 NaH_2PO_4, 1.2 $MgSO_4$, 2.5 $CaCl_2$, 26 $NaHCO_3$, and 10 dextrose. This solution was heated to 31°C and oxygenated using a gas mixture containing 95% O_2-5% CO_2. Mitral and granule cells were identified based on their morphology and location within the olfactory bulb slices visualized using infrared differential interference contrast (IR-DIC) microscopy (Axioskop 1 FS upright microscope, Carl Zeiss, Thornwood, NY). Both mitral and granule cells were recorded in current-clamp mode using a whole cell patch-clamp amplifier (Axopatch 1D amplifier; Molecular Devices, Sunnyvale, CA). Recording pipettes were generally filled with the following internal solution (in mM): 140 K-methylsulfate, 8

NaCl, 0.2 EGTA, 10 HEPES, 4 Mg-ATP, 0.3 Na_3GTP, and 10 phosphocreatine-Tris (pH 7.3, 290 mOsm). Only granule cells with resting membrane potentials more hyperpolarized than –75 mV were included in this study. In some experiments, we increased the Ca buffering capacity of the internal solution by replacing 0.2 EGTA with 10 BAPTA plus 1.3 $CaCl_2$ (calculated $[Ca]_{in}$ = 53 nM). Pipette resistances using these internal solutions were ~3 MΩ for mitral cells and 5 MΩ for granule cells. All drugs were obtained from Sigma (St. Louis, MO). Pooled data are shown as means ± SE. Unless stated otherwise, we used two-tailed paired *t*-test for statistical comparisons between two sets of pooled data and unpaired *t*-test for comparisons between different experimental data sets.

Fluorescent Ca signals were recorded using a custom photodiode-based detector. In these experiments, we replaced the 0.2 mM EGTA normally present in the internal solution with 0.2 mM Oregon Green 488 BAPTA-1 (OG1; Invitrogen, Eugene, OR). All electrical signals were low-pass filtered at 5 kHz and then digitally sampled at 10 kHz into a Windows NT-based PC computer using an ITC-18 A/D converter (Instrutech, Port Washington, NY) controlled by custom Igor-Pro (WaveMetrics, Lake Oswego, OR) programs. Fluorescent signals initially were converted into fractional changes ($\Delta F/F$). These signals were corrected for bleaching using a linear regression and digitally filtered (band-pass, 30 Hz to 10 kHz).

Intracellular current injection, including sine wave stimulation and simulated inhibitory postsynaptic potential (IPSP), was performed by the ITC-18 A/D converter and custom Igor-Pro programs. The injected current pulse used to trigger transient discharges in granule cells was either 250 or 500 ms in duration. The current injected for the oscillation of membrane potentials in granule and mitral cells was given by the following equation

$$I(t) = I_{max} \times 0.5 \times \{\cos[2\pi(ft + 0.5)] + I\} \qquad (1)$$

where f is the oscillation frequency, I_{max} is the oscillation amplitude of the injected current. The oscillation frequency was 2 Hz in most experiments. I_{max} was adjusted in each experiment so that the peak of the membrane potential oscillation was just subthreshold. Because the injected oscillatory current was inward, the membrane potential returned to near rest (typically -75 to -80 mV) at the hyperpolarizing extent of each cycle. In the mode in which our custom software operated, the ITC-18, episode duration was limited by the hardware buffer size to 10–15 s. This limitation affected both our ability to record data as well as to generate oscillating current stimuli.

We adopted a uniform metric, P_{Cycle}, to assess the effectiveness of transient stimuli to trigger persistent activity in oscillation granule cells. In most experiments, we calculated this metric using the mean spike probability in cycles 10–11 ($P_{Cycle10-11}$) or in cycles 21–22 ($P_{Cycle21-22}$) when we manipulated the experimental conditions after persistent firing was established. This metric, which varied from 0 to 1, was calculated from the average probability that those specific oscillation cycles triggered at least one action potential (AP). We measured the amplitude of the underlying membrane potential envelope in oscillatory (Figs. 1*C2* and 3, *A2* and *B3*) and half-cycle (Fig. 4) responses after APs were removed using a moving median filter (10-ms window). Traces were visually inspected to ensure that all APs were removed by the filtering procedure. Plots of the relative change (ΔV_m) in the depolarizing or hyperpolarizing extent of the underlying membrane potential oscillation were generated by subtracting the mean peak voltage reached during four oscillation cycles before the transient discharge.

Extracellular stimuli in external plexiform layer (EPL) in the olfactory bulb were delivered through bipolar tungsten electrodes (electrode tips separation was 125 μm; WPI, Sarasota, FL) positioned 300–500 μm from the mitral cell body. Electrical stimuli (300–800 μA intensity and 200 μs duration) were delivered through a stimulus isolation unit (WPI). The current injected for the simulated IPSP was given by the alpha-function

$$I(t) = A \times \alpha t \times \exp(-\alpha t) \qquad (2)$$

where α is the inverse of the decay time constant, and A is the coefficient representing the IPSP amplitude.

Computer simulations

Each granule or mitral cell was represented by a two-compartment model that included a single somatic and a single dendritic compartment; passive electrotonic spread between compartments was modeled using the discrete version of the cable equation (Traub and Miles 1991). All voltage-gated currents in our models were defined using the Hodgkin-Huxley formalism. We employed a set of five purely voltage-dependent currents in our granule cell model [fast Na current, delayed rectifier K current, transient (A-type) K current, low-threshold (T-type) Ca current, and high-threshold (P/N-type) Ca current] and one calcium-dependent current (calcium- and voltage-dependent nonselective cation current). Intracellular Ca dynamics in granule cells were calculated using a pool model (De Schutter and Smolen 1998). We employed a set of three voltage-dependent currents in our mitral cell model (fast Na current, delayed rectifier K current, and slowly inactivating K current). Dendritic compartments in granule and mitral cells form reciprocal synapses that mediate recurrent inhibition (Isaacson and Strowbridge 1998). We simulated these synaptic interactions using an AMPAR-based excitatory current in the synapse from mitral to granule cell and GABA$_A$R-based inhibitory current in the synapse from the granule to mitral cell. These synaptic currents were modeled by first-order kinetic schemes (Destexhe et al. 1998).

Detailed information about these models is described in the supplementary materials section.[1]

All simulations were performed using a custom-made program written in C++ (Visual C++ 6.0, Microsoft, Redmond, WA) on a PC running the Windows 2000 operating system (Microsoft). We used IgorPro 4.0 (WaveMetrics) as a graphic user interface (GUI) to the C-based model; the main simulation program and GUI were connected through a custom Igor XOP-file. We used a fourth-order Runge-Kutta method (Mascagni and Sherman 1998) to numerically solve ordinary differential equations using a time step of 0.04 ms.

RESULTS

Persistent activity in oscillating granule cells

We initially addressed the functional consequences of slow oscillations in olfactory bulb neurons by applying a 2-Hz sinusoidal current stimulus to granule cells in the presence of 1–2 μM carbachol. This stimulus induced a membrane potential oscillation without any significant buildup or rectification during 10- to 15-s recording episodes. Surprisingly, we found that this oscillating subthreshold response could be converted into persistent spiking activity after a transient discharge evoked during a single oscillation cycle (Fig. 1*B*; $n = 9$). Granule cells generated single action potentials near the most depolarized phase in most oscillation cycles after the transient stimulus. Persistent activity was maintained throughout the remainder of the acquired episode (typically ~10 s; Fig. 1*C*), although occasionally individual oscillation cycles failed to trigger an action potential (Fig. 1*B*). The average probability of triggering an action potential on the oscillation cycles 10 and 11 ($P_{Cycle10-11}$) using this protocol was 0.78 ± 0.13 ($n = 9$ cells). The transient stimulus also increased the depolarizing extent of the underlying membrane potential oscillation (from -53.7 ± 2.7 to -42.4 ± 2.9 mV; $P < 0.01$; $n = 9$) and slightly, but significantly, reduced the hyperpolarizing oscillation extent (from -80.8 ± 0.9 to -78.6 ± 1.4 mV; $P < 0.05$; Fig. 1*C2*).

Persistent spiking activity required activation of muscarinic acetylcholine receptors (mAChRs) in granule cells. In granule cells recorded in control ACSF, transient discharges caused a depression in the evoked membrane potential oscillation that lasted 5–7 s ($P_{Cycle10-11} = 0$; Fig. 1*D*). The same transient discharge that caused a hyperpolarizing response in control conditions triggered persistent firing after bath application of 1 μM CCh (see Fig. 1*D*, *bottom trace*; 9 of 9 cells tested). In the absence of a subthreshold oscillation, transient discharges failed to trigger persistent activity in granule cells held near rest even in CCh ($n = 9$; data not shown). Persistent activity was triggered reliably by transient discharges consisting of ≥ 5 Na spikes; weaker depolarizing stimuli that triggered only a single Na spike did not evoke persistent spiking (Fig. 1*E*; $n = 6$). Persistent spiking activity appeared to be an all-or-none response to the transient stimulus. We never observed spiking activity that lasted for only a few cycles except under certain experimental conditions (see following text). Interrupting the membrane oscillation abolished the persistent activity; restoring the oscillation 5 s later did not recover the spiking activity (Fig. 2*A1*). Similar results were observed in all seven experiments using this protocol, as shown in the summary plot in Fig. 2*A2* (mean $P_{Cycle22-23} = 0$ after pausing oscillation

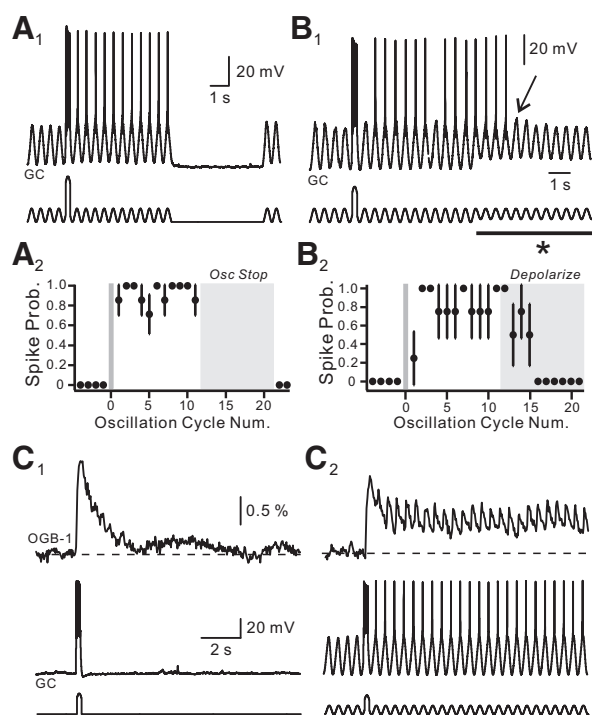[1] The online version of this article contains supplemental data.

FIG. 2.   Modulation of persistent firing. *A1*: halting the membrane potential oscillation abolishes persistent spiking activity; restarting the oscillation fails to recover spiking activity. *A2*: summary plot of spiking probability vs. oscillation cycle number for 7 experiments using the same protocol shown in *A1*. *B1*: reducing the hyperpolarizing extent of the membrane potential oscillation (by ~9 mV) gradually abolishes the persistent spiking activity and the low-threshold spikes (↓) initiated on each oscillation cycle. Horizontal bar with * indicates time period when oscillation amplitude was reduced. *B2*: summary plot for 4 experiments using the protocol in *B1*. *C1*: transient discharge causes a short-term increase in intracellular [Ca] in granule cells. *C2*: persistent spiking activity in oscillating granule cells is associated with a sustaining increase in intracellular [Ca]. Action potentials truncated.

vs. $P_{Cycle10-11} = 0.93 \pm 0.08$; $P < 0.01$; paired *t*-test). Persistent activity was not dependent on this specific oscillation frequency but also could be evoked by transient discharges superimposed on somewhat faster membrane potential oscillations (5 Hz; data not shown) within the physiological range of the sniffing behavior (Freeman and Skarda 1985). Because this form of persistent activity is dependent on a computer-generated oscillating current stimulus, hardware buffer size limitations prevented us from defining the duration of this firing mode (beyond the ~10 s responses shown in Figs. 1 and 2).

Persistent spiking in granule cells was not caused by synaptic or network effects of the transient discharge because persistent spiking could be evoked in the presence of a mixture of blockers of ionotropic glutamate and GABA receptors (10 μM NBQX, 50 μM D-2-amino-5-phosphonovaleric acid, and 50 μM picrotoxin; $n = 3$; data not shown). Instead persistent spiking activity appeared to result from the facilitation of small, regenerative, intrinsic responses on each oscillation cycle that triggered action potentials. High-gain records of granule cell recordings (Fig. 1*D, right*) and analysis of median-filtered membrane potential records (Fig. 1*C2*) showed that the depolarizing extent of the membrane potential oscillation was enhanced after the transient discharge. Persistent firing occurred because these facilitated depolarizing responses reached AP threshold. Facilitated responses to the membrane potential oscillation were occasionally isolated in oscillation cycles that

failed to trigger an AP (see Fig. 1*B*). The hyperpolarizing extent of the membrane potential oscillation in CCh only slightly (2.2 ± 0.9 mV) affected by the transient discharge, suggesting that persistent activity was not associated with a large change in input resistance.

These initial data are consistent with a model in which the transient discharge enhances an intrinsic inward current that is repeatedly activated on the depolarizing phases of the membrane potential oscillation. However, persistent activity also may be caused by a hyperpolarizing shift in the action potential threshold. To discriminate between these hypotheses, we decreased the hyperpolarizing extent of the sinusoidal current oscillation after persistent activity was established. If the transient discharge evoked persistent spiking activity by lowering the action potential threshold, presumably by increasing K current inactivation, this manipulation should enhance the persistent spiking activity by further reducing K currents. By contrast, the same manipulation would be expected to block persistent activity if this firing mode was mediated by facilitated low-threshold Ca spikes because the underlying T-type Ca currents likely require phasic hyperpolarizations to de-inactivate (Jahnsen and Llinas 1984). As shown in Fig. 2*B1*, we found that decreasing the hyperpolarizing extent of the membrane potential oscillation blocked persistent spiking activity (4 of 4 cells tested; mean $P_{Cycle21-22} = 0$ with reduced hyperpolarizing extent vs. $P_{Cycle10-11} = 0.88 \pm 0.14$; $P < 0.01$; paired *t*-test; Fig. 2*B2*). Interestingly, persistent firing was not initially blocked; rather it was maintained for three to four cycles after the transient stimulus. Facilitated depolarizing responses were evident immediately after Na spiking ceased, and these facilitated responses gradually decayed over the next four to five cycles (Fig. 2*B; n = 4*). These results suggest that persistent spiking was not caused by a reduced AP threshold but, rather, required enhanced inward currents triggered on each oscillation cycle.

We used Ca photometry to test whether persistent spiking was associated with a sustained increase in intracellular Ca concentration. We found that transient discharges alone caused a marked increase in intracellular Ca that decayed completely within 2–3 s (Fig. 2*C1;* decay $\tau = 880 \pm 190$ ms). By contrast, persistent spiking triggered by the same discharge in oscillating granule cells was associated with a sustained elevation in intracellular Ca (Fig. 2*C2*). Similar results were observed in four granule cells. No elevation in somatic [Ca] was observed when the oscillating current stimulus was tested by itself (data not shown; $n = 4$).

We next asked if persistent spiking required a sustained elevation in intracellular Ca in granule cells. As illustrated in Fig. 3*A1*, we found that the low-voltage activated (LVA) Ca channel antagonist nickel (100 μM) reversibly blocked persistent spiking activity in granule cells ($P_{Cycle20-21} = 0$ in Ni vs. 0.80 ± 0.22 in control; $n = 5$; $P < 0.05$; paired *t*-test). In the presence of Ni, transient discharges caused a facilitation of the response to the next few oscillation cycles, often triggering one to two APs. Bath application of Ni also prevented the majority of the long-lasting increase in the depolarizing extent of the underlying membrane potential oscillation (ΔV_m for the depolarizing oscillation extent at cycle 23 = 2.5 ± 0.6 mV in Ni vs. 11.8 ± 1.0 mV in control). As shown in the summary plot in Fig. 3*A2*, only an initial, short-term facilitation in the depolarizing extent of the membrane potential oscillation remained in
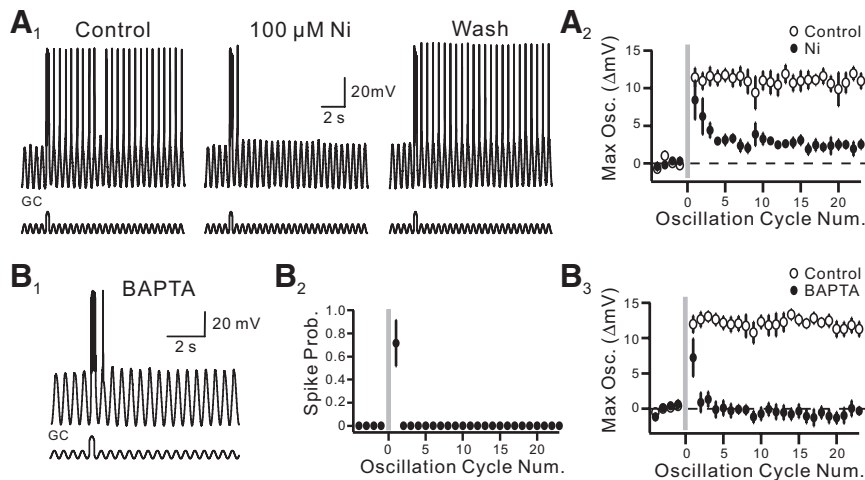
FIG. 3. Calcuim-dependent responses mediate persistent spiking activity. *A1*: nickel (100 μM) reversibly blocks persistent spiking activity initiated by transient discharges in oscillating granule cells. *A2*: effect of transient discharge on depolarizing oscillation extent in control ($\circ$) and Ni ($\bullet$) experiments. *B1*: transient discharges fail to trigger persistent spiking in granule cells filled with 10 mM bis-(*o*-aminophenoxy)-*N,N,N′,N′*-tetraacetic acid (BAPTA). *B2*: summary plot of spike probability per cycle for 7 experiments using the same protocol shown in *B1*. *B3*: effect of transient discharge on depolarizing oscillation extent in control ($\circ$) and BAPTA-filled ($\bullet$) granule cells.

Ni-treated slices. Finally, we tested whether persistent firing required sustained elevations in intracellular Ca by stimulating transient discharges in oscillating granule cells loaded with BAPTA (Fig. 3*B1*). This stimulus paradigm failed to trigger persistent spiking in all seven BAPTA-loaded granule cells tested (mean $P_{Cycle20-21} = 0$; Fig. 3*B2*). The same protocol evoked persistent spiking activity in nine of nine granule cells, recorded with a control internal solution containing 0.2 mM EGTA (mean $P_{Cycle20-21} = 0.78 \pm 0.13$; significantly different from BAPTA experiments; $P < 0.01$; unpaired *t*-test). Transient discharges triggered only very short-term enhancements, typically lasting one cycle, in the underlying oscillatory voltage response when intracellular Ca was strongly buffered with BAPTA (ΔV_m for the depolarizing oscillation extent at cycle 23 = -0.3 ± 0.5 mV; Fig. 3*B3*). These data suggest that maintenance of persistent spiking activity requires a Ca-activated inward current, whereas the low-threshold Ca spike functions primarily to amplify the depolarizing phase of each oscillatory cycle. This hypothesis provides an explanation for the short-term facilitation in the depolarizing oscillation extent after the low-threshold spike (LTS) is blocked by Ni (Fig. 3*A2*).

Mechanism of persistent spiking in granule cells

Persistent firing appears to result from the interplay between short-term responses to the initiating discharge and the dynamic conditions imposed by the membrane potential oscillation. We next sought to define the short-term consequences of the transient discharge using simpler, nonoscillatory stimuli that reproduce only one half-cycle of the periodic stimuli. Under control conditions, transient discharges caused a large reduction in the voltage responses to this stimulus (mean response change = -6.4 ± 2.2 mV; $n = 5$; Fig. 4*A*), likely reflecting the inhibitory effect of the afterhyperpolarization (AHP). Bath application of CCh abolished this inhibition, resulting in a second response that was now greater than the control response and reached threshold to trigger an action potential (Fig. 4*A, middle*; mean response change = $+12.1 \pm$ 1.3 mV; $n = 9$ cells; significantly different from control; $P <$ 0.01; unpaired *t*-test). This result is consistent with the recent demonstration that activation of M1 cholingeric receptors converts the normal granule cell AHP response into an afterdepo-

larization (ADP) (Pressler et al. 2007). The ADP response appears to be mediated by a Ca-activated, nonselective cation current (I_{CAN}) and can be mimicked by uncaging Ca in granule cells (Pressler et al. 2007).

Several mechanisms might be responsible for the potentiation of the second response in CCh. Most simply, the increased amplitude of the second response might reflect the summation of the ADP response with the passive response to the current injection. However, a modified stimulus that prevented the membrane potential from fully repolarizing after the transient discharge reduced the facilitation of the second response in CCh (Fig. 4*A, right*; mean response change = $+1.7 \pm 0.5$ mV; $n = 7$; significantly different from CCh; $P < 0.01$; unpaired *t*-test). This result is inconsistent with the ADP summation model and suggests that the transient discharge might have a second action, independent of the I_{CAN} current, which facilitated inward currents in granule cells. We tested this hypothesis using similar current injection protocols in BAPTA-loaded granule cells (conditions under which the ADP response is blocked). We found that transient discharges still potentiated depolarizing responses in the absence of Ca-signaling (Fig. 4*B*; Ca spike amplitude = 4.1 ± 1.8 mV with depolarizing step alone vs. 14.7 ± 0.7 mV when the step was preceded by a discharge; $P < 0.01$; $n = 5$; Ca spike amplitude measured after APs were removed using a moving median filter). The potentiation of depolarizing responses in BAPTA-loaded granule cells also was dependent on full repolarization of the membrane potential after the transient discharge (Fig. 4*B, right*; Ca spike amplitude 3.1 ± 0.9 mV; significantly different from control cells with a preceding discharge; $P < 0.01$). These results strongly suggest that the transient discharge facilitates regenerative currents in granule cells triggered by subsequent stimuli. Insufficient repolarization after the transient discharge likely prevents de-inactivation of the underlying intrinsic inward currents. Given the relatively hyperpolarized threshold needed to elicit these potentiated responses (near AP threshold), it is likely that they are mediated by LVA Ca channels. Consistent with the behavior of T-type Ca currents in other neurons (Jahnsen and Llinas 1984), we found that granule cells generated rebound spikes (Fig. 4*C*), and the rebound LTS responses were potentiated (and often triggered an action potential) when preceded by a transient discharge (see also Egger et al. 2003, 2005). The amplitude of the underlying
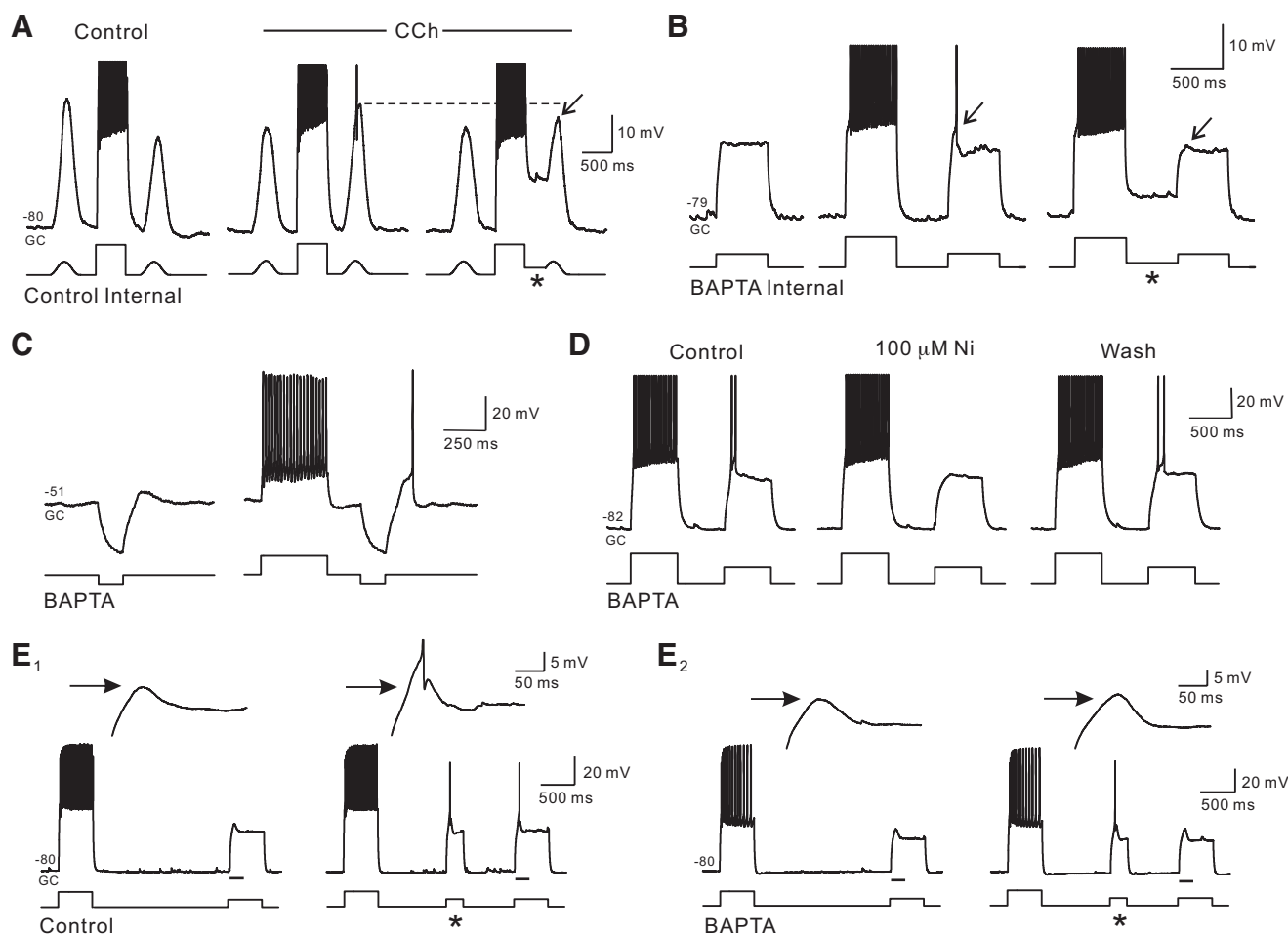
FIG. 4.   Transient discharges facilitate low-threshold Ca spikes in granule cells. *A*: response to an isolated half-cycle sinusoidal oscillation is reduced after a transient discharge in control conditions. The response to the same stimulus is facilitated relative to predischarge response in CCh (1 μM) and triggers an action potential (*middle*). The magnitude of facilitation is reduced when the membrane potential is not allowed to fully repolarize after the transient discharge (*right*). Initial membrane potential indicated above trace. *B*: transient discharges also facilitate low-threshold spikes on subsequent depolarizing current steps in BAPTA (10 mM)-loaded granule cells. These low-threshold spikes are not initiated when the membrane potential does not fully repolarize after the discharge (*right*). *C*: transient discharges also facilitate rebound spikes in response to brief hyperpolarizing steps in BAPTA-loaded granule cells. *D*: low-threshold spikes modulated by transient discharges are blocked by 100 μM nickel in BAPTA-loaded granule cells. *E1*: facilitation of low-threshold Ca spikes is enhanced when a brief suprathreshold current step (*) is applied between the transient discharge and the test response in control granule cells. *E2*: this enhancement is not observed in BAPTA-loaded granule cells. All responses in *B–E* recorded in CCh. Action potentials truncated in *A, B, D,* and *inset* in *E1*.

rebound Ca spike increased from 6.1 ± 1.0 to 17.3 ± 3.7 mV when the hyperpolarizing step was preceded by a discharge (statistically different; $P < 0.05$; paired *t*-test; $n = 3$). Also, the LVA Ca channel antagonist nickel (100 μM) reversibly blocked the potentiated response to depolarizing test stimuli in BAPTA-loaded granule cells (Fig. 4*D*; $n = 3$).

Our results suggest that transient discharges have two distinct and experimentally separable effects on CCh-treated granule cells: a Ca-dependent ADP response and a Ca-independent process that facilitates low-threshold Ca spikes. We employed the three-pulse protocol illustrated in Fig. 4*E* to test how these mechanisms interact to enable Ca-activated I_{CAN} currents to facilitate low-threshold Ca spikes in granule cells. We adjusted the amplitude of the final test pulse so that a small Ca spike was evoked only when the test pulse was preceded by a transient discharge (Fig. 4*E1*). We found that including an additional depolarizing pulse between the initial discharge and the test pulse increased the amplitude of the Ca spike evoked by the final test pulse in five of five cells tested (from 4.6 ± 1.5 to

13.9 ± 1.1 mV; $P < 0.01$; paired *t*-test; $n = 5$). This potentiating effect was observed only when the middle pulse triggered an action potential and was not found in parallel experiments with BAPTA-loaded granule cells (Fig. 4*E2*; 4.4 ± 2.2 without middle pulse vs. 6.7 ± 1.0 mV with middle pulse; $P > 0.05$; paired *t*-test; $n = 4$). Together, these results suggest a model in which persistent spiking activity is initiated by a Ca-independent mechanism that facilitates low-threshold Ca spikes and is maintained by the inward current generated by the Ca-dependent ADP.

Rebound spikes in mitral cells

How does persistent activity in GABAergic granule cells affect mitral cells? Mitral cells are known to generate rebound spikes to hyperpolarizing stimuli (Balu and Strowbridge 2007; Desmaisons et al. 1999; Schoppa 2006). We found that both hyperpolarizing current pulses (Fig. 5*A*; $n = 15$) and inhibitory postsynaptic potentials (Fig. 5*B*; $n = 3$) could trigger rebound

A

-41
MC

10 mV
100 ms

-47

B

20 mV
200 ms
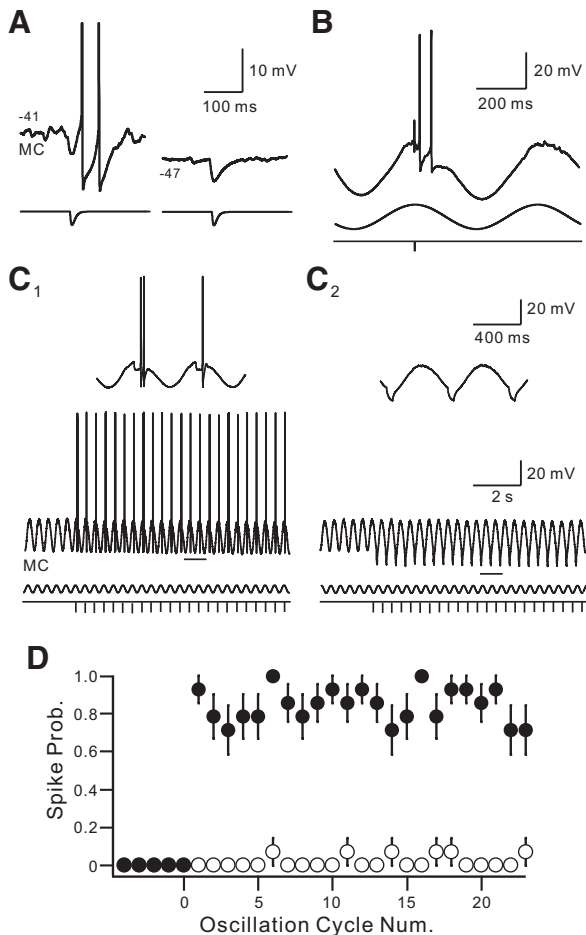
C₁

C₂

20 mV
400 ms

20 mV
2 s

MC

D

FIG. 5. Inhibitory postsynaptic potentials (IPSPs) trigger rebound spikes in mitral cells. *A*: simulated IPSP waveform current injections elicit rebound Na spikes in mitral cells held near firing threshold. *B*: synaptically evoked IPSPs also elicit rebound spikes in oscillating mitral cells when they are triggered near the maximal oscillatory depolarization. *C1*: repetitive rebound Na spikes evoked by 2-Hz trains of hyperpolarizing current pulses in oscillating mitral cells when each stimulus coincided with the maximal oscillatory depolarization. *C2*: no rebound spiking occurred in response to the same hyperpolarizing input when the stimulus train was delayed by 1 half-cycle (each hyperpolarizing pulse coinciding with the most hyperpolarized extend of the membrane potential oscillation). Horizontal bars indicate areas expanded in traces above. *D*: summary plot of spike probability vs. oscillation cycle showing results from 14 experiments using in-phase hyperpolarizing inputs (●) and anti-phase inputs (○).

Na spikes in mitral cells. Rebound spikes were generated reliably only within a relatively narrow range of membrane potentials (-41 to -47 mV in the cell shown in Fig. 5*A*). The narrow voltage range over which hyperpolarizations triggered rebound spikes suggests that inhibitory postsynaptic potential (IPSP)-spike coupling should be sensitive to the phase relations of the driving oscillation and to the IPSP in oscillating mitral cells. We found this was the case with robust rebound responses triggered only by IPSPs that occurred near the most depolarized phase of the oscillation (Fig. 5*C*). No action potentials were triggered by the same IPSPs when they occurred during the hyperpolarizing phase. Tonic firing in oscillating mitral cells could be induced by synchronizing the inhibitory stimuli with the peak depolarization evoked by the sinusoidal current injection (Fig. 5*C1*; mean $P_{Cycle20-21} = 0.89 \pm 0.08$; $n = 14$). No spikes were evoked when this phase relationship was shifted $180°$ so that the hyperpolarizing pulses

coincided with the most hyperpolarized extent of the oscillation (Fig. 5*C2*; $P_{Cycle20-21} = 0$; $n = 14$; significantly different from peak depolarization experiments; $P < 0.01$; paired *t*-test). Results from these experiments are summarized in the plot shown in Fig. 5*D* and suggest that inhibitory inputs could trigger rebound spikes in mitral cells when both cell types are subject to the same slow oscillatory drive (e.g., during rhythmic sniffing) (Cang and Isaacson 2003; Margrie et al. 2003).

Persistent activity in simulated mitral granule cell pairs

We used computer simulations to examine whether these cellular mechanisms support persistent activity in synaptically connected mitral/granule cell pairs. We first constructed a two-compartment granule cell model that incorporated six voltage-dependent currents in both soma and dendrite compartments (see supplementary methods section for details). By adjusting the current densities of these conductances, we arrived at a parameter set that reproduced the experimentally recorded responses of granule cells to weak and strong depolarizing current steps (Fig. 6*A*). The same model produced a small Ca spike in response to the offset of a hyperpolarizing current pulse (Fig. 6*B*). Preceding this current pulse with a transient discharge potentiated the low-threshold Ca spike (compare with Fig. 4*C*). The model also reproduced the facilitation of Ca spikes in response to depolarizing pulses. These LTS responses were facilitated by prepulses in simulations that did not include any Ca-dependent currents. When Ca-dependent processes were enabled, simulated granule cells generated Ca- and voltage-dependent ADP responses (ADP at -60 mV was 2.4 mV and 0 mV at -80 mV). The currents mediating the slow afterhyperpolarization were not included in the simulation, thereby mimicking the experimental conditions when CCh was included in the bath solution.

Simulated granule cells displayed persistent spiking activity in response to the sinusoidal current injection protocol used in Figs. 1 and 2. Consistent with our experimental results, persistent activity in simulated granule cells required the combination of a transient suprathreshold stimulus and a constant membrane potential oscillation (Fig. 6*C, left*). Neither component, when presented by itself, elicited persistent activity. Persistent activity required the activation of both simulated LVA Ca channels and Ca-dependent ADP responses. Blockade of either current, or preventing intracellular [Ca] to increase after the transient discharge, abolished persistent spiking activity in our model (data not shown). The effect of reducing the hyperpolarizing extent of the membrane potential oscillation on persistent activity (see Fig. 2*B1*) was reproduced in the computer model, where it was reflected in reduced de-inactivation of LVA Ca currents (see I_T monitor signal in Fig. 6*C, right*). Persistent firing, but not the transient discharge itself, was also associated with a sustained elevation in intracellular [Ca] (Fig. 6*D*) consistent with our experimental results (see Fig. 2*C2*).

Mitral cells were simulated using a two-compartment model that incorporated three voltage-dependent conductances. The presence of a slowly inactivating K current, resembling the current produced by the $K_v1.3$ potassium channel subunits (Fadool and Levitan 1998; Fadool et al. 2004), enabled simulated mitral cells to generate rebound spikes similar to those shown in Fig. 5. Rebound spikes could be generated in re-
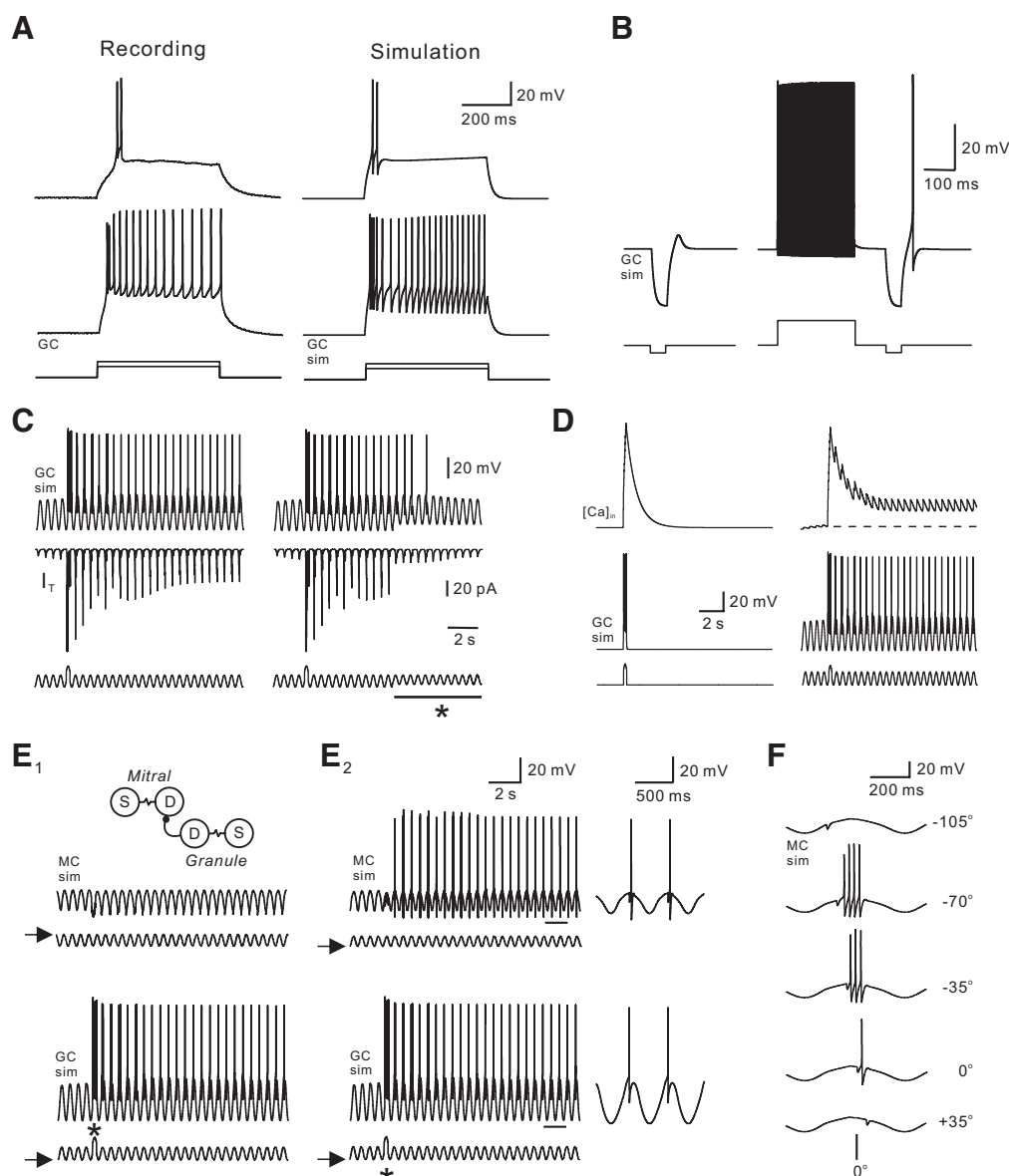
FIG. 6. Computational model of persistent spiking activity in granule cells. *A*: comparison of responses to weak and strong depolarizing steps in a granule cell (*left*) and in a 2-compartment simulation of a granule cell (*right*). *B*: transient discharges facilitate rebound low-threshold Ca spikes in simulated granule cells. *C*: transient discharges trigger persistent firing in oscillating simulated granule cells. Same stimulus protocol shown in Fig. 1*B*. *Bottom traces*: amplitude of simulated low-threshold Ca current. Hyperpolarizing extent of membrane oscillation reduced on *right traces* during period indicated by horizontal bar and *. *D*: dendritic compartment Ca dynamics in response to a transient discharge in control (*left*) or oscillating (*right*) simulated granule cells. *E*: persistent spiking in granule cells induces spiking in coupled mitral cells. Simulation included an inhibitory synapse from granule cell to the mitral cell. Transient depolarizing stimulus applied to simulated granule cell (*). Persistent spiking was evoked in the mitral cell when the sinusoidal current oscillations were synchronized in both cells (*E2*); no spiking activity occurred in the mitral cell when the mitral cell oscillation was delayed by a half cycle (*E1*). Horizontal bars indicate region of voltage traces expanded on *right*. *F*: example responses of oscillating simulated mitral cells to an IPSP delivered at different times during the membrane potential oscillation. The phase advance (negative numbers) or retardation (positive numbers) of the IPSP relative to the oscillation peak is indicated to the right of each trace. Simulated I_{CAN} current was disabled for traces in *B*.

sponse to both hyperpolarizing voltage steps (data not shown) and to simulated IPSPs (Fig. 6, *E* and *F*) when the mitral cell was held near firing threshold. Simulated granule-cell-to-mitral-cell monosynaptic IPSPs decayed with a time constant of 20 ms, similar to the experimentally determined kinetics of mitral cell IPSPs evoked by extracellular stimulation (24.2 ± 7.5 ms; $n = 3$). The mitral-cell-to-granule-cell excitatory postsynaptic potential (EPSP) used in the model was based on a simulated AMPAR-mediated current that decayed with a

time constant of 2.2 ms (Isaacson 2001). NMDAR-mediated currents were not included in these simulations to simplify interpretation of these results.

Persistent spiking activity in one granule cell initiated correlated spiking in a unidirectionally coupled mitral cell. As shown in Fig. 6*E*, activation of the coupled mitral cell was dependent on the synchronization between the membrane potential oscillations in both cells. (Mitral and granule cells were not reciprocally connected in these simulations because the

excitatory synaptic connection from the mitral cell to the granule cell was disabled.) With no phase lag between the mitral and granule cell membrane potential oscillations, spiking activity in granule cells evoked IPSPs in mitral cells 3 ms after the peak oscillatory depolarization. In response, the mitral cell typically generated a single rebound action potential (see expansion in Fig. 6E2). The magnitude of the mitral cell response depended strongly on when the IPSP was evoked during each oscillation cycle. IPSPs that occurred 100 ms before the peak oscillatory depolarization (70° phase-advanced) produced the largest responses (Fig. 6F). Increasing the phase-advance of the IPSP by >135° or retarding the IPSP by >35° abolished rebound spiking.

Reciprocally connected mitral cell/granule cell pairs generated robust persistent spiking activity. Persistent activity occurred in both mitral and granule cells when the fast AMPAR synapse between mitral and granule cells was enabled in the simulation (Fig. 7A). In the reciprocally connected model,

persistent activity could be initiated by a transient depolarization of the mitral cell (simulating the normal disynaptic activation of granule cells after olfactory nerve activity). This stimulus resulted in a large, summated EPSP and intracellular Ca accumulation in the granule cell. When reciprocally connected, both mitral and granule cells generated multiple action potentials on each oscillation cycle. Intracellular [Ca] also stabilized at a higher concentration in reciprocally connected granule cells than in granule cells that did not receive synaptic input from mitral cells (compared with Fig. 6D). As in unidirectionally coupled pairs, persistent spiking activity in reciprocally coupled pairs was dependent on synchronization of the sinusoidal current injection in each cell.

The robustness of persistent activity in reciprocally connected simulated olfactory bulb networks was caused by the excitatory component of the reciprocal synaptic connection (from the mitral cell to the granule cell.) The typical multiple-spike response during each oscillation cycle was reduced to a
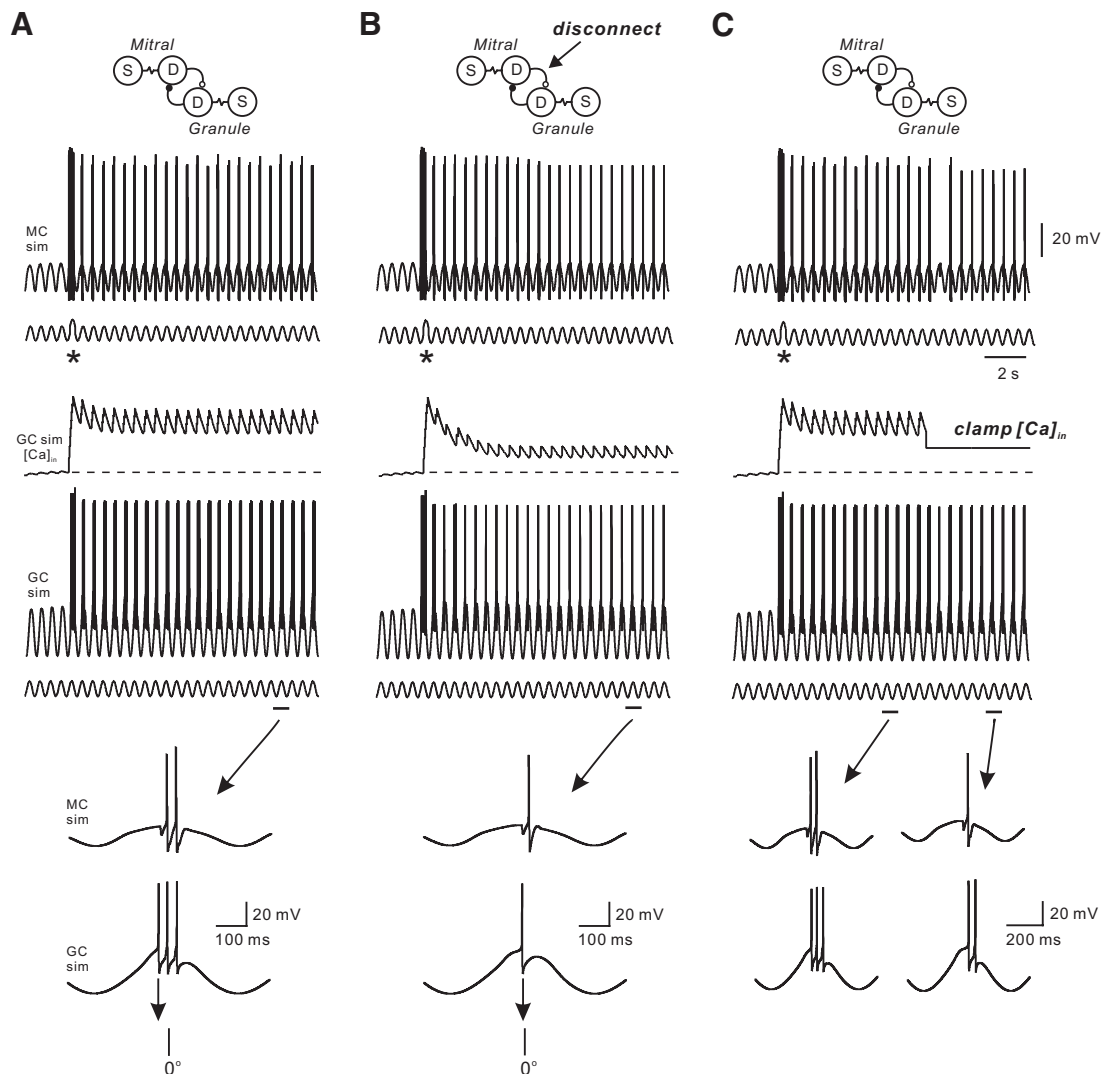

FIG. 7. Persistent spiking activity in reciprocally connected mitral cell/granule cell models. A: persistent activity is enhanced when the excitatory synapse from the mitral cell to the granule cell is enabled (compare with Fig. 5E2). Persistent activity initiated by a transient discharge in the mitral cell (*). Persistent activity induces a sustained elevation in intracellular Ca in the simulated granule cell (middle). Horizontal bars indicate regions that are expanded in faster sweeps shown below. B: persistent spiking activity is reduced in reciprocally connected mitral/granule cell pairs when the mitral cell-to-granule cell synapse was disabled immediately after the transient discharge. Under this condition, the persistent spike was associated with a smaller sustained elevation in intracellular Ca in the simulated granule cell. C: clamping the intracellular Ca concentration to a similar steady-state concentration shown in B reduces persistent spiking activity.

single action potential when this synaptic connection was disabled immediately after the transient discharge (Fig. 7*B*). The increased spiking evoked in both cell types in the reciprocally connected model was caused by multiple effects of the mitral-cell-to-granule-cell synapse. First, when this synapse was present, spiking activity in the mitral cell generated an additional source of depolarization in the granule cell. This synaptic input potentiated low-threshold Ca-spiking in the granule cell, leading to elevated intracellular [Ca] and increased I_{CAN} current. The effect of the elevated [Ca] in reciprocally connected granule cells is illustrated in Fig. 7*C*. In this experiment, intracellular [Ca] was manually clamped to the same steady-state concentration found in unidirectionally connected granule cells (from Figs. 6*D* and 7*B*). This manipulation converted the multiple-spike granule cell response on each oscillation cycle into a single action potential and made the mitral cell response less reliable. The facilitating effect of this excitatory synapse on mitral cells was more complex. As shown in Fig. 7*A*, the IPSPs evoked in reciprocally connected mitral cells were phase-advanced by 23° (32 ms for a 2-Hz oscillation), relative to the peak oscillatory depolarization. By contrast, IPSPs evoked in unidirectionally connected mitral cells occurred slightly after the peak depolarization (delayed by 4°; see Fig. 7*B*). It is likely that this phase-advance, rather than the increased IPSP amplitude, led to the larger mitral cell discharge through the mechanism shown in Fig. 6*F*.

DISCUSSION

Our findings suggest a novel mechanism for generating persistent spiking activity in phasically active neurons. Persistent activity in olfactory granule cells can be triggered by a single, brief depolarization, and it results from the repetitive activation of low-threshold Ca spikes. This mechanism also requires a second phasic input to granule cells to de-inactivate the T-type current that underlies low-threshold Ca spikes in these neurons. Persistent activity is maintained by a Ca-sensitive afterdepolarization, likely mediated by I_{CAN} current. Our computer simulations suggest that persistent activity in inhibitory granule cells can entrain synaptically connected mitral cells if both cell types receive synchronized oscillatory input. This form of persistent activity in the olfactory bulb may reflect a generalizable mechanism for synchronizing the firing of subpopulations of reciprocally connected neurons during attentionally regulated repetitive behaviors, such as sniffing.

Persistent activity mediated by intrinsic currents in granule cells

Our results suggest that persistent spiking in granule cells arises from the interaction between two intrinsic responses: a voltage-dependent afterdepolarization and a low-threshold Ca spike (Fig. 8). Afterdepolarizations have been reported previously in frog (Hall and Delaney 2002) and rat (Pressler et al. 2007) granule cells. Afterdepolarizations in both studies were Ca and voltage dependent and were reduced by flufenamic acid, suggesting that they are mediated by a nonselective cation current (I_{CAN}) (Haj-Dahmane and Andrade 1998, 1999). Using the Ca chelator BAPTA, we could differentiate the two Ca-mediated responses in granule cells (ADPs and low-threshold Ca spikes) and determine that the inward current mediated by
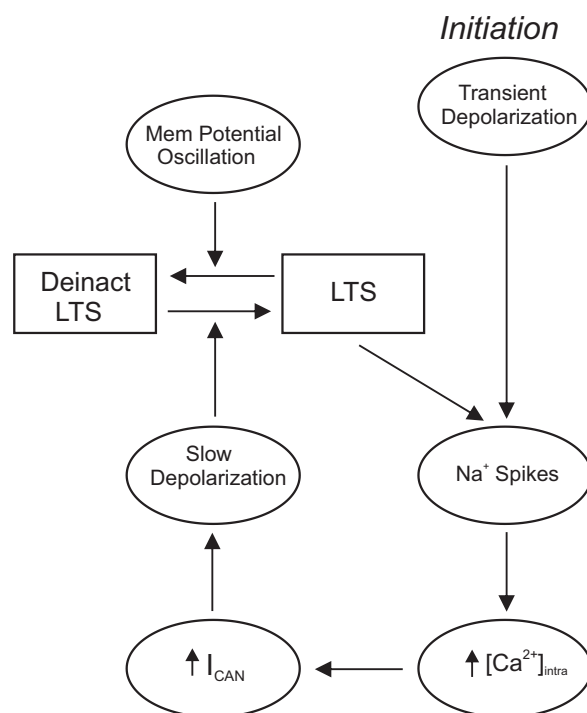

FIG. 8. Summary diagram of the proposed model of persistent spiking activity in granule cells. Persistent spiking results from facilitated low-threshold Ca spikes (LTS) that are activated by the combination of the sinusoidal membrane potential oscillation and the Ca-actived nonselective cation current (I_{CAN}). Activation of the I_{CAN} current reflects previous Na spiking activity. The current underlying the LTS is de-activated during the hyperpolarizing extent sinusoidal membrane potential oscillation.

I_{CAN} contributes to the maintenance of persistent firing in granule cells. In the slice preparation, I_{CAN}-mediated ADPs are tonically blocked by much larger AHP responses. As in other brain regions (Egorov et al. 2002; Haj-Dahmane and Andrade 1999), muscarinic receptor activation suppresses the AHP in granule cells, revealing the ADP response (Pressler et al. 2007). The presence of two opposing currents (AHP and ADP) in granule cells raises the possibility that persistent firing activity in the olfactory bulb is regulated by centrifugal cholingeric afferents in vivo.

The accentuated depolarizing responses to sinusoidal current injections after transient depolarizations reflect the generation of low-threshold Ca spikes. Regenerative LTS responses were inactivated by slight depolarization, suggesting that they are mediated by T-type Ca currents (Avery and Johnston 1996; Crunelli et al. 1989; Randall and Tsien 1997). Consistent with this hypothesis, we find that LTS responses are abolished in low-Ca/high-Mg ACSF (data not shown) and by 100 μM nickel. At this concentration, nickel blocks predominately T- and R-type Ca currents (Bournaud et al. 2001; Randall and Tsien 1997). The relatively hyperpolarized threshold we find for the LTS in granule cells (approximately −50 mV) is consistent with the activation of T-type Ca channels. Our results also are consistent with several recent studies demonstrating low-threshold Ca responses in granule cells (Egger et al. 2003, 2005; Pinato and Midtgaard 2005). Granule cells also generate LTS responses after hyperpolarizing steps, paralleling findings in other neurons where these rebound spikes reflect de-inactivation, followed by activation of T-type Ca currents (Jahnsen and Llinas 1984; Wilcox et al. 1988). Fur-

thermore, our results are consistent with an in situ hybridization study demonstrating that granule cells express high levels of mRNA transcripts for the $Ca_V3.1$–3.3 subunits (Talley et al. 1999) that encode T-type Ca channels (Cribbs et al. 1998; Perez-Reyes et al. 1998).

We find that the T-current mediating the LTS response is reduced under resting conditions in granule cells and that this tonic inhibition can be reversed by prior depolarization. Although we did not explore the mechanism of this modulation in detail, we do not believe that it is mediated by intracellular Ca signaling because we observe modulation in BAPTA-loaded granule cells. It is possible that the transient depolarization reduces K currents active near rest that prevent regenerative LTS responses. Schoppa and Westbrook (1999) reported that granule cells express I_A-type K currents that are blocked by 4-aminopyridine (4-AP). In addition to regulating recurrent dendrodendritic inhibition, these I_A currents may regulate persistent spiking activity by controlling LTS activation. Alternatively, the depolarization may affect signaling cascades that modulate T-type Ca channels directly.

Based on our experimental findings, we propose a model in which persistent spiking in granule cells results from the interaction among T-type Ca channels, the I_{CAN} current, and a phasic current stimulus. The Ca influx during the transient depolarization leads to a small ADP response that brings the next oscillation cycle to threshold for triggering a low-threshold Ca spike. In our experiments, it is the depolarizing LTS response, not the ADP response, that enables the granule cell to generate action potentials. The ADP response, by contrast, appears to operate over multiple oscillation cycles and contributes to the tonic depolarization of the granule cell during persistent firing. The T-type Ca current underlying the low-threshold Ca spike is "recycled" (through de-inactivation) by the hyperpolarizing phase of the sinusoidal membrane potential oscillation and another LTS response can be triggered on the next oscillation cycle. The hyperpolarizing phase of the membrane potential oscillation is passive because we injected an inward sinusoidal current waveform (i.e., the hyperpolarizing peak is reached when no current is applied). Because granule cells rest at relatively hyperpolarized membrane potentials, it is possible that T-type Ca currents are de-inactivated in the inter-sniff interval in vivo though a similar passive mechanism.

This sequence of events occurs in the granule cell computational model that we developed (incorporating both the I_{CAN} current and T-type Ca channels) in response to the stimulus protocols used in our experiments. This hypothesis explains why persistent spiking is abolished by manipulations that either reduce I_{CAN} activation (BAPTA-loading) or inhibit T-type Ca currents (nickel or preventing complete repolarization during the oscillatory response). Single action potentials can maintain persistent spiking in oscillating granule cells but cannot initiate this activity. The larger depolarizations required to initiate persistent spiking probably reflect the other, as yet undefined, steps required to remove the tonic inhibition of LTS responses in granule cells. In our model, the additional depolarization generated by the low-threshold Ca spike represents the critical step that enables persistent firing in granule cells. The contribution of the Ca influx through low-threshold Ca channels to the ADP response is less certain because granule cells also contain high-threshold Ca channels (Isaacson 2001) that are likely to be activated by action potentials triggered by LTS responses.

Reverberating activity in synaptically connected olfactory bulb neurons

We find that mitral cells can generate rebound Na spikes after hyperpolarizing stimuli such as IPSPs consistent with previous direct demonstrations of rebound activity after hyperpolarizing current injections (Balu and Strowbridge 2007; Desmainsons et al. 1999) and synchronous mitral cell discharges evoked by inhibitory postsynaptic potentials (Schoppa 2006). Recent work on the mechanism of rebound discharges in mitral cells (Balu and Strowbridge 2007) suggests that these responses are regulated by two opposing conductances: slowly inactivating K currents and subthreshold Na currents. These currents interact to generate a narrow window, near firing threshold, where hyperpolarizing stimuli trigger rebound spikes. One consequence of this combination of currents is that rebound spikes are triggered more reliably by weak hyperpolarizing stimuli than by large-amplitude hyperpolarizations (Balu and Strowbridge 2007). This behavior may help to synchronize mitral discharges on specific phases of the slow inspiration-linked oscillation. We successfully simulated rebound spiking in mitral cells, using a combination of I_A, Na current and a Kv1.3-like K current known to be expressed in mitral cells (Balu et al. 2004; Fadool and Levitan 1998; Fadool et al. 2000, 2004). Interestingly, mitral and granule cells appear to generate rebound activity through different cellular mechanisms: T-type Ca currents in granule cells and subthreshold Na currents in mitral cells (Balu and Strowbridge 2007).

The ability of persistent activity in granule cells to induce firing in coupled mitral cells depends critically on the phase synchronization between the granule cell spikes and the mitral cell subthreshold oscillation. If both cell types receive synchronized sinusoidal oscillations, IPSPs are evoked slightly after the maximal oscillatory depolarization, and they generally trigger a single action potential. However, if the simulated mitral and granule cells are reciprocally connected, as they normally are through reciprocal dendrodendritic synapses (Isaacson and Strowbridge 1998; Jahr and Nicoll 1980, 1982; Rall et al. 1966), persistent activity in both cell types becomes more robust, and multiple action potentials are triggered on each oscillation cycle. The granule cell response is facilitated by the additional depolarization from the mitral cell EPSP. The mitral cell response is enhanced largely because the granule cell IPSP now arrives earlier during each oscillation cycle (i.e., it is phase-advanced) and, therefore, evokes a larger rebound depolarization. We required relatively large synaptic conductances to achieve transfer of persistent spiking activity from granule cells to mitral cells in our two-cell network. It is likely that smaller unitary synaptic conductances would be required to evoke persistent firing in mitral cells if we employed more complex network models, incorporating convergence from multiple granule cells onto individual mitral cells.

Functional significance of persistent activity in the olfactory bulb

We employed a set of experimental manipulations (sinusoidal subthreshold stimuli, transient intracellular discharges, and muscarinic receptor agonists) in this study to demonstrate the propensity of olfactory bulb granule cells to generate persistent spiking activity. But are these artificial manipulations related to

normal physiological activity in the olfactory bulb? We find that sinusoidal membrane potential oscillations enable persistent firing through two separate actions. First, the rising phase of the oscillation contributes to the depolarization required to trigger the LTS response. During persistent spiking, this phasic depolarization is enhanced by the ADP triggered by Ca entry during previous cycles. The second action occurs during the falling phase of the oscillation when the T-type Ca current inactivated during the last LTS response is de-inactivated. In principle, other forms of phasic stimuli, such as trains of large, temporally summating EPSPs granule cells receive during sniffing, could accomplish the same effects. It is likely that these phasic, disynaptic EPSPs contribute to the 2-Hz oscillations recorded in olfactory bulb field potentials (Freeman and Skarda 1985). It is not known, however, whether the slow rhythmic field potentials recorded during sniffing reflect simply these sensory-driven synaptic responses or whether these synaptic responses are reinforced by intrinsic and/or local circuit properties of olfactory bulb neurons. The mechanism we propose, which enables correlated spiking in both granule and mitral cells, depends critically on the synchronization of the phasic stimuli to both cell types. This synchronization occurs during normal breathing, when both granule and mitral cells fire during the same phase of the 2-Hz population oscillation (Ravel et al. 1987).

The transient depolarization we used to initiate persistent firing provides an initial, large Ca influx and enhances the inward currents that mediate LTS responses. Both effects could be accomplished by the direct, sensory-evoked EPSP onto granule cells (after being relayed through mitral cells) or through the activation of centrifugal excitatory synaptic inputs to granule cells (Balu et al. 2007; Kishi et al. 1984; Orona et al. 1984). The requirement for cholinergic input reflects the need to suppress the AHP response in granule cells (Pressler et al. 2007). It is possible that the large AHP conductance in granule cells tonically inhibits persistent activity, allowing periods of persistent activity to be gated by activity in cholinergic neurons in the basal forebrain. Most of the cholinergic inputs to the rat olfactory bulb arise from neurons in the horizontal limb of the diagonal band (Zaborszky et al. 1986) and terminate predominately in the granule cell layer (Broadwell and Jacobowitz 1976; Luskin and Price 1983; Macrides et al. 1981). Based on our results, we predict that granule cell firing in response to olfactory stimulation will be enhanced after activation of cholinergic basal forebrain neurons and that this facilitation will be dependent on the I_{CAN} current in granule cells.

REFERENCES

Adrian ED. Olfactory reactions in the brain of the hedgehog. *J Physiol* 100: 159–473, 1942.

Avery RB, Johnston D. Multiple channel types contribute to the low-voltage-activated calcium current in hippocampal CA3 pyramidal neurons. *J Neurosci* 16: 5567–5582, 1996.

Balu R, Strowbridge BW. Opposing inward and outward conductances regulate rebound spiking in olfactory bulb mitral cells. *J Neurophysiol* 97: 1959–1968, 2007.

Balu R, Pressler RT, Strowbridge BW. Multiple mechanisms of synaptic excitation of olfactory bulb granule cells. *J Neurosci* 27: 5621–5632, 2007.

Balu R, Larimer P, Strowbridge BW. Phasic stimuli evoke precisely timed spikes in intermittently discharging mitral cells. *J Neurophysiol* 92: 743–753, 2004.

Bournaud R, Hidalgo J, Yu H, Jaimovich E, Shimahara T. Low-threshold T-type calcium current in rat embryonic chromaffin cells. *J Physiol* 537: 35–44, 2001.

Broadwell RD, Jacobowitz DM. Olfactory relationships of the telencephalon and diencephalon in the rabbit. III. The ipsilateral centrifugal fibers to the olfactory bulbar and retrobulbar formations. *J Comp Neurol* 170: 321–345, 1976.

Cang J, Isaacson JS. In vivo whole-cell recordings of odor-evoked synaptic transmission in the rat olfactory bulb. *J Neurosci* 23: 4108–4116, 2003.

Chaput MA. EOG responses in anesthetized freely breathing rats. *Chem Senses* 25: 695–701, 2000.

Chaput M, Holley A. Single unit responses of olfactory bulb neurones to odour presentation in awake rabbits. *J Physiol* 76: 551–558, 1980.

Compte A, Brunel N, Goldman-Rakic PS, Wang XJ. Synaptic mechanisms and network dynamics underlying spatial working memory in a cortical network model. *Cereb Cortex* 10: 910–923, 2000.

Cribbs LL, Lee JH, Yang J, Satin J, Zhang Y, Daud A, Barclay J, Williamson MP, Fox M, Rees M, Perez-Reyes E. Cloning and characterization of alpha1H from human heart, a member of the T-type Ca^{2+} channel gene family. *Circ Res* 83: 103–109, 1998.

Crunelli V, Lightowler S, Pollard CE. A T-type Ca^{2+} current underlies low-threshold Ca^{2+} potentials in cells of the cat and rat lateral geniculate nucleus. *J Physiol* 413: 543–561, 1989.

De Schutter ED, Smolen P. Calcium dynamics in large neuronal models. In: *Methods in Neuronal Modeling* (2nd ed.), edited by Koch C, Segev I. Cambridge, MA: MIT Press, 1998, p. 211–250.

Desmaisons D, Vincent JD, Lledo PM. Control of action potential timing by intrinsic subthreshold oscillations in olfactory bulb output neurons. *J Neurosci* 19: 10727–10737, 1999.

Destexhe A, Mainen ZF, Sejnowski TJ. Kinetic models of synaptic transmission. In: *Methods in Neuronal Modeling,* edited by Koch C, Segev I. Cambridge, MA: MIT Press, 1998.

Destexhe A, McCormick DA, Sejnowski TJ. Thalamic and thalamocortical mechanisms underlying 3 Hz spike-and-wave discharges. *Prog Brain Res* 121: 289–307, 1999.

Eeckman FH, Freeman WJ. Correlations between unit firing and EEG in the rat olfactory system. *Brain Res* 528: 238–244, 1990.

Egger V, Svoboda K, Mainen ZF. Mechanisms of lateral inhibition in the olfactory bulb: efficiency and modulation of spike-evoked calcium influx into granule cells. *J Neurosci* 23: 7551–7558, 2003.

Egger V, Svoboda K, Mainen ZF. Dendrodendritic synaptic signals in olfactory bulb granule cells: local spine boost and global low-threshold spike. *J Neurosci* 25: 3521–3530, 2005.

Egorov AV, Hamam BN, Fransen E, Hasselmo ME, Alonso AA. Graded persistent activity in entorhinal cortex neurons. *Nature* 420: 173–178, 2002.

Everitt BJ, Robbins TW. Central cholinergic systems and cognition. *Annu Rev Psychol* 48: 649–684, 1997.

Fadool DA, Levitan IB. Modulation of olfactory bulb neuron potassium current by tyrosine phosphorylation. *J Neurosci* 18: 6126–6137, 1998.

Fadool DA, Tucker K, Phillips JJ, Simmen JA. Brain insulin receptor causes activity-dependent current suppression in the olfactory bulb through multiple phosphorylation of Kv1.3. *J Neurophysiol* 83: 2332–2348, 2000.

Fadool DA, Tucker K, Perkins R, Fasciani G, Thompson RN, Parsons AD, Overton JM, Koni PA, Flavell RA, Kaczmarek LK. Kv1.3 channel gene-targeted deletion produces "Super-Smeller Mice" with altered glomeruli, interacting scaffolding proteins, and biophysics. *Neuron* 41: 389–404, 2004.

Freeman WJ, Skarda CA. Spatial EEG patterns, non-linear dynamics and perception: the neo-Sherringtonian view. *Brain Res* 357: 147–175, 1985.

Goldman-Rakic PS. Cellular basis of working memory. *Neuron* 14: 477–485, 1995.

Haj-Dahmane S, Andrade R. Ionic mechanism of the slow afterdepolarization induced by muscarinic receptor activation in rat prefrontal cortex. *J Neurophysiol* 80: 1197–1210, 1998.

Haj-Dahmane S, Andrade R. Muscarinic receptors regulate two different calcium-dependent non-selective cation currents in rat prefrontal cortex. *Eur J Neurosci* 11: 1973–1980, 1999.

Hall BJ, Delaney KR. Contribution of a calcium-activated non-specific conductance to NMDA receptor-mediated synaptic potentials in granule cells of the frog olfactory bulb. *J Physiol* 543: 819–834, 2002.

Isaacson JS. Mechanisms governing dendritic gamma-aminobutyric acid (GABA) release in the rat olfactory bulb. *Proc Natl Acad Sci USA* 98: 337–342, 2001.

Isaacson JS, Strowbridge BW. Olfactory reciprocal synapses: dendritic signaling in the CNS. *Neuron* 20: 749–761, 1998.

Jahnsen H, Llinas R. Ionic basis for the electro-responsiveness and oscillatory properties of guinea-pig thalamic neurons in vitro. *J Physiol* 349: 227–247, 1984.

Jahr CE, Nicoll RA. Dendrodendritic inhibition: demonstration with intracellular recording. *Science* 207: 1473–1475, 1980.

Jahr CE, Nicoll RA. An intracellular analysis of dendrodendritic inhibition in the turtle in vitro olfactory bulb. *J Physiol* 326: 213–234, 1982.

Kishi K, Mori K, Ojima H. Distribution of local axon collaterals of mitral, displaced mitral, and tufted cells in the rabbit olfactory bulb. *J Comp Neurol* 225: 511–526, 1984.

Luskin MB, Price JL. The topographic organization of associational fibers of the olfactory system in the rat, including centrifugal fibers to the olfactory bulb. *J Comp Neurol* 216: 264–291, 1983.

Macrides F, Chorover SL. Olfactory bulb units: activity correlated with inhalation cycles and odor quality. *Science* 175: 84–87, 1972.

Macrides F, Davis BJ, Youngs WM, Nadi NS, Margolis FL. Cholinergic and catecholaminergic afferents to the olfactory bulb in the hamster: a neuroanatomical, biochemical, and histochemical investigation. *J Comp Neurol* 203: 495–514, 1981.

Margrie TW, Schaefer AT. Theta oscillation coupled spike latencies yield computational vigor in a mammalian sensory system. *J Physiol* 546: 363–374, 2003.

Mascagni MV, Sherman AS. Numerical methods for neuronal modeling. In: *Methods in Neuronal Modeling* (2nd ed.), edited by Koch C, Segev I. Cambridge, MA: MIT Press, 1998.

McCormick DA, Bal T. Sleep and arousal: thalamocortical mechanisms. *Annu Rev Neurosci* 20: 185–215, 1997.

Orona E, Rainer EC, Scott JW. Dendritic and axonal organization of mitral and tufted cells in the rat olfactory bulb. *J Comp Neurol* 226: 346–356, 1984.

Perez-Reyes E, Cribbs LL, Daud A, Lacerda AE, Barclay J, Williamson MP, Fox M, Rees M, Lee JH. Molecular characterization of a neuronal low-voltage-activated T-type calcium channel. *Nature* 391: 896–900, 1998.

Pinato G, Midtgaard J. Dendritic sodium spikelets and low-threshold calcium spikes in turtle olfactory bulb granule cells. *J Neurophysiol* 93: 1285–1294, 2005.

Pressler RT, Inoue T, Strowbridge BW. Cholinergic modulation of afterpotentials and firing modes of granule cells in the olfactory bulb. *J Neurosci* 27: 10969–10981, 2007.

Pressler RT, Strowbridge BW. Blanes cells mediate persistent feedforward inhibition onto granule cells in the olfactory bulb. *Neuron* 49: 889–904, 2006.

Rall W, Shepherd GM, Reese TS, Brightman MW. Dendrodendritic synaptic pathway for inhibition in the olfactory bulb. *Exp Neurol* 14: 44–56, 1966.

Randall AD, Tsien RW. Contrasting biophysical and pharmacological properties of T-type and R-type calcium channels. *Neuropharmacology* 36: 879–893, 1997.

Ravel N, Caille D, Pager J. A centrifugal respiratory modulation of olfactory bulb unit activity: a study on acute rat preparation. *Exp Brain Res* 65: 623–628, 1987.

Ravel N, Elaagouby A, Gervais R. Scopolamine injection into the olfactory bulb impairs short-term olfactory memory in rats. *Behav Neurosci* 108: 317–324, 1994.

Ravel N, Vigouroux M, Elaagouby A, Gervais R. Scopolamine impairs delayed matching in an olfactory task in rats. *Psychopharmacology* 109: 439–443, 1992.

Schoppa NE. Synchronization of olfactory bulb mitral cells by precisely timed inhibitory inputs. *Neuron* 49: 271–283, 2006.

Schoppa NE, Westbrook GL. Regulation of synaptic timing in the olfactory bulb by an A-type potassium current. *Nat Neurosci* 2: 1106–1113, 1999.

Shepherd GM, Greer CA. Olfactory Bulb. In: *Synaptic Organization of the Brain* (4th ed.), edited by Shepherd GM. New York: Oxford, 1998, p. 159–204.

Sobel EC, Tank DW. Timing of odor stimulation does not alter patterning of olfactory bulb unit activity in freely breathing rats. *J Neurophysiol* 69: 1331–1337, 1993.

Stopfer M, Bhagavan S, Smith BH, Laurent G. Impaired odour discrimination on desynchronization of odour-encoding neural assemblies. *Nature* 390: 70–74, 1997.

Talley EM, Cribbs LL, Lee JH, Daud A, Perez-Reyes E, Bayliss DA. Differential distribution of three members of a gene family encoding low voltage-activated (T-type) calcium channels. *J Neurosci* 19: 1895–1911, 1999.

Traub RD, Miles R. *Neural Networks of the Hippocampus.* Cambridge: Cambridge Univ. Press, 1991.

Wang XJ. Synaptic reverberation underlying mnemonic persistent activity. *Trends Neurosci* 24: 455–463, 2001.

Welker WE. Analysis of sniffing of the albino rat. *Behaviour* 22: 223–244, 1964.

Wilcox KS, Gutnick MJ, Christoph GR. Electrophysiological properties of neurons in the lateral habenula nucleus: an in vitro study. *J Neurophysiol* 59: 212–225, 1988.

Zaborszky L, Carlsen J, Brashear HR, Heimer L. Cholinergic and GABAergic afferents to the olfactory bulb in the rat with special emphasis on the projection neurons in the nucleus of the horizontal limb of the diagonal band. *J Comp Neurol* 243: 488–509, 1986.